Vector field path following and obstacle avoidance singularity mitigation via look-ahead flight envelope

First A. Author* and Second B. Author Jr.†
Business or Academic Affiliation 1, City, State, Zip Code

Unmanned Aerial Vehicles conventionally navigate by following a series of pre-planned waypoints that may have to be re-planned when flying in a dynamic environment or encountering previously unknown obstacles. Waypoints are generally planned off-line and relayed to the UAV, taking up time and autopilot communication resources. Attractive path following and repulsive obstacle avoidance vector fields have been summed together to produce UAV guidance that follows pre-planned paths and avoids obstacles without the need to re-plan. Summing attractive and repulsive vector fields may produce small regions of null guidance, called singularities, which could potentially lead to trap situations. An investigation into singularity mitigation by vector field weight parameterization is presented.

I. Nomenclature

UAV = Unmanned Aerial Vehicle
VF = Vector Field
VFF = Virtual Force Field
LVF = Lyapunov Vector Field
GVF = Goncalves Vector Field

II. Introduction

Unmanned Aerial Vehicles (UAV)s are pilotless aircraft used by military, police, and civilian communities for tasks such as reconnaissance, damage assessment, surveying, and target tracking [1, 2]. Tasks can be performed by a single UAV or cooperate with a team of other air, ground, or marine vehicles [3–5]. UAVs are ideal for remote data collection due to their low cost, endurance, and reduced risk to human life. Data can be collected by loitering the aircraft around an area of interest (AOI) or along a sensor path, such as a road or tree-line. Missions for collecting data are typically pre-planned on a remote ground station where an obstacle free and flyable path is generated. Constraints such as optimizing sensor converge may be considered when planning [6]. Typically paths are deconstructed into a series of discrete waypoints that the UAV navigates to through the use of a line-of-sight guidance. While navigating the pre-planned path previously unknown obstacles may be discovered and a new obstacle free path may have to be generated, which may be difficult or impossible if the UAV is out of radio range. Directing the UAV to temporarily deviate from the planned path to avoid an obstacle may be accomplished with an on board guidance such as Potential Field or path following Vector Field. Potential field is a popular solution to both path planning and guidance problems in obstacle rich environments, however suffers from several limitations including local minima, oscillations, and may cause excess deviation from the desired sensor line. Vector field converges and circulates a pre-defined path and may be summed with additional repulsive vector fields to produce an obstacle avoidance guidance. Avoidance fields may be further optimized to reduce the deviation from a sensor path by modifying convergence and circulation scalar weights. Additionally, summing attractive and repulsive fields may result in singularities, small regions of null guidance that can produce trap situations. The contribution of this work is to provide an optimized vector field guidance for path following and obstacle avoidance as well as providing a method for identifying vector field singularities. First, the Dubin's UAV model will be presented followed by a description of waypoint guidance, potential field, and vector field. A method for singularity detection in summed vector field will be discussed, followed by a modified obstacle avoidance vector field.

*Insert Job Title, Department Name, Address/Mail Stop, and AIAA Member Grade (if any) for first author.
†Insert Job Title, Department Name, Address/Mail Stop, and AIAA Member Grade (if any) for second author.

Simulations comparing the discussed guidance methods were conducted along with a multirotor demonstration of the improved vector field.

A. Dubins Vehicle

UAVs traveling at constant altitude and velocity and with a limited turn rate can be simplified as a Dubin's vehicle that flies in straight line and circular arcs. It was assumed that an on-board controller accepts heading commands and produces vehicle roll to change the vehicles heading. The position $\overrightarrow{X}$ at time t is calculated from the integral of the velocity vector $\overrightarrow{U}$. The vehicle has a constant velocity magnitude u_{uav} at a heading θ. Heading is an input from a guidance system, such as waypoint, potential field, or vector field.

$$\overrightarrow{U}(t) = u_{uav} \begin{bmatrix} cos(\theta(t)) \\ sin(\theta(t)) \end{bmatrix} \tag{1}$$

$$\overrightarrow{X}(t) = \overrightarrow{U} dt + \overrightarrow{X}(t-1) \tag{2}$$

$$\dot{\theta} \leq 20 deg/s \tag{3}$$

B. Waypoint Guidance

Waypoint guidance aligns the vehicle with the currently active waypoint that lies along a pre-planned path. Paths are typically generated off-line and can be optimized for shortest distance traveled and further refined to be flyable for a particular vehicle. Paths may also be optimized to produce flight patterns that increase sensor coverage of an area of interest [6]. If an obstacle lies along that sensor path, the UAV must avoid the obstacle but also return back to the sensor path such that a minimal length of the path is missed during data collection. Waypoints placed on the outside the radius of the obstacle can direct a UAV around an obstacle and back onto the desired sensor path. Obstacles discovered during flight that lie along the pre-planned path may require a new path to be planned, requiring communication with the ground station. If a new path is not relayed to the UAV in time the vehicle may fail to avoid the obstacle. Additionally, if a new path is generated, it will most likely require that waypoints be placed some distance away from the obstacle's edge to accommodate the wayoints detection radius, increasing both deviation and time spent away from original path. An example of waypoints planned around an obstacle is shown in Figure 1 below.

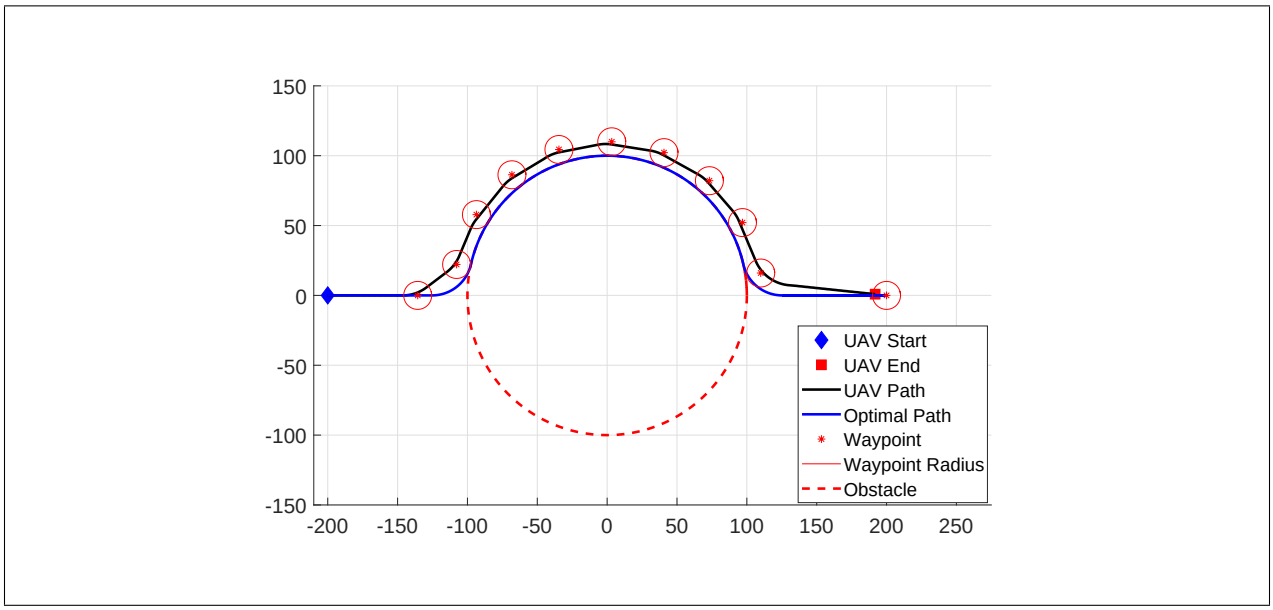

Fig. 1 Simulated Fixed Wing UAV Traversing Waypoints Around Circular Obstacle

It would be beneficial to include obstacle avoidance into a UAVs guidance system to remove the need to communicate with the ground station and path re-planning.

C. Potential Field

Potential field is based on the principle of artificial attractive and repulsive forces acting on a point mass to guide a system to a desired goal while avoiding static and dynamic obstacles [7]. Goals states are represented as an attractive force that pulls a point mass in the direction of minimal energy while obstacles are represented as repulsive forces that act locally to push the point mass away. Potential field also is capable of acting as a path and trajectory planning algorithm [8], possibly eliminating the off-board path planner. An example of potential field can be found in [9–11] which allowed for real time goal seeking with obstacle avoidance on a mobile ground robot equipped with ultrasonic sensors. The robot located at (x_0, y_0) is attracted towards a a goal with constant magnitude force $\overrightarrow{F_t}$ located at (x_t, y_t) and a distance d_t from the robot. In the immediate area of the robot, an active window exists which records integer certainty values inside discrete cells. Cells containing an obstacle provide a repulsive force $\overrightarrow{F_{i,j}}$ opposite in direction to the line-of-sight from vehicle to cell location (x_i, y_j), where (i, j) represents the cell index, F_{cr} is a constant repulsive force, W the vehicle's width, $C_{i,j}$ a cell's certainty, and $d_{i,j}$ the distance to the center of the cell with respect to robots center.

$$\overrightarrow{F_{i,j}} = \frac{F_{cr} W^n C_{i,j}}{d_{i,j}^n} \left(\frac{x_i - x_0}{d_{i,j}} \hat{x} + \frac{y_i - y_0}{d_{i,j}} \hat{y} \right) \tag{4}$$

The total repulsive force exerted on the robot is determined by summing the active cells, shown in Equation 5

$$\overrightarrow{F_r} = \sum_{i,j} \overrightarrow{F_{i,j}} \tag{5}$$

$$\overrightarrow{F_t} = F_{ct} \left(\frac{x_t - x_0}{d_t} \hat{x} + \frac{y_t - y_0}{d_t} \hat{y} \right) \tag{6}$$

Summing together attractive and repulsive forces produce a vector that can be used for heading guidance, shown in Equation 7.

$$\overrightarrow{R} = \overrightarrow{F_r} + \overrightarrow{F_t} \tag{7}$$

Major drawbacks to potential field were identified in [11] consisting of local minimum and oscillations in corridors. The local minimum problem occurs when closely spaced obstacle's potential combine to produce a well on the descent gradient where a pre-mature stable point is reached. Proposed solutions to local minimum include object clustering and virtual waypoint method [12], virtual escaping route [13], and use of navigation functions [14]. Oscillations in potential field were studied in [15] and [16].

In addition to local minimum and oscillations, potential field may not be ideal for providing guidance to return to a sensor path after avoiding an obstacle. Once the obstacle has been avoided, the attractive goal will direct the UAV in a straight path which may not lie along the sensor line. Guidance that follows an explicit path, deviates when necessary to avoid obstacles, and returns back to the explicit path quickly can be accomplished with path following vector fields.

D. Vector Field Guidance

Vector fields produce continuous heading guidance that asymptotically converges and circulates a path. A comparison between vector field and waypoint guidance techniques was presented in [17] where each method was evaluated based on its complexity, robustness, and accuracy. The vector field model produced guidance that was both robust to external wind disturbances while maintaining a low cross track error. The two most prominent methods for generating vector fields in literature consist of the Lyapunov [18–23] and Goncalves [24–27] method. Lyapunov vector fields for converging and following straight and circular paths were described in [18]. Straight and circular path vector fields can be selectively activated throughout flight to form more complex paths, shown in [18–20, 28]. Lyapunov vector field for curved path following was presented in [23] which may allow for more complex paths and eliminates the need to switch between vector fields.

E. GVF

The Gonvalves Vector Field (GVF) method produces a similar field, however has several advantages over LVFs. GVF produces an n-dimensional vector field that converges and circulates to both static and time varying paths. Additionally,

convergence, circulation, and time-varying terms that make up the GVF are decoupled from each other allowing for easy weighting of the total field. GVFs converge and circulate at the intersection, or level set, of $n-1$ dimensional implicit surfaces ($\alpha_i : \mathbb{R}^n \rightarrow \mathbb{R} | i = 1, ..., n-1$). The integral lines of the field are guaranteed to converge and circulate the level set when two conditions are met: 1) the implicit surface functions are positive definite and 2) have bounded derivatives.

The total vector field $\overrightarrow{V}$ is calculated by:

$$\overrightarrow{V} = G\nabla V + H \wedge_{i=1}^{n-1} \nabla\alpha_i - LM(\alpha)^{-1}a(\alpha) \tag{8}$$

or in component form:

$$\overrightarrow{V} = G\overrightarrow{V}_{conv} + H\overrightarrow{V}_{circ} + L\overrightarrow{V}_{tv} \tag{9}$$

where $\overrightarrow{V}_{conv}$ produces vectors perpendicular to the path, $\overrightarrow{V}_{circ}$ produces vectors parallel to the path, and $\overrightarrow{V}_{tv}$ is a feed-forward term that produces vectors accounting for a time varying path.

Convergence is calculated by:

$$\vec{V}_{conv} = \nabla V \tag{10}$$

where scalar G is multiplied by the gradient of the definite potential function V:

$$V = -\sqrt{{\alpha_1}^2 + {\alpha_2}^2} \tag{11}$$

$$\nabla V = \begin{bmatrix} \frac{dV}{dx} \\ \frac{dV}{dy} \\ \frac{dV}{dz} \end{bmatrix} \tag{12}$$

Circulation is calculated by taking the wedge product of the gradients of the surface functions:

$$\vec{V}_{circ} = \wedge_{i=1}^{n-1} \nabla\alpha_i \tag{13}$$

In the case of ($n = 3$) the wedge product simplifies as the cross product:

$$\vec{V}_{circ} = \nabla\alpha_1 \times \nabla\alpha_2 \tag{14}$$

The feed-forward time-varying component is calculated by:

$$\vec{V}_{tv} = M^{-1}a \tag{15}$$

where,

$$M = \begin{bmatrix} \nabla\alpha_1^T \\ \nabla\alpha_2^T \\ (\nabla\alpha_1 \times \nabla\alpha_2)^T \end{bmatrix} \tag{16}$$

$$a = \begin{bmatrix} \frac{\partial\alpha_1}{\partial t} & \frac{\partial\alpha_2}{\partial t} & 0 \end{bmatrix}^T \tag{17}$$

Intersecting two flat planes ($\alpha_1 = z, \alpha_2 = x$) produces a GVF that converges and circulates a straight path, shown in Figure 3.

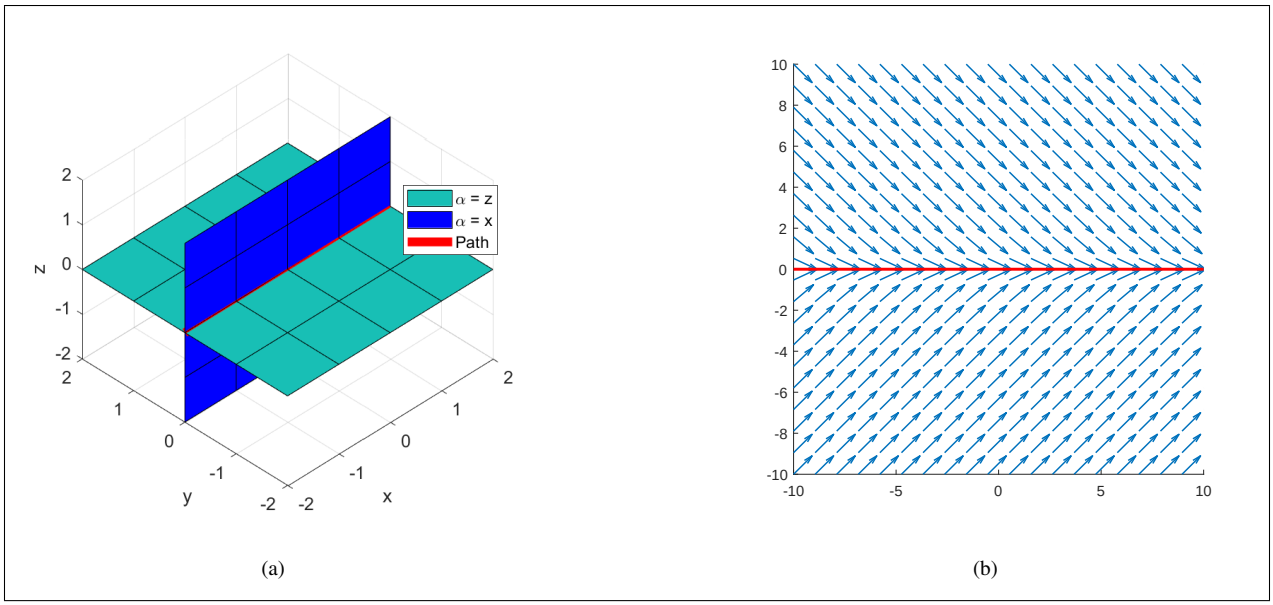

Fig. 2 GVF converging and circulating straight path

A GVF for converging and circulating a circular path can be produced by intersecting a plane and a cylinder ($\alpha_1 = z, \alpha_2 = x^2 + y^2 - r^2$).

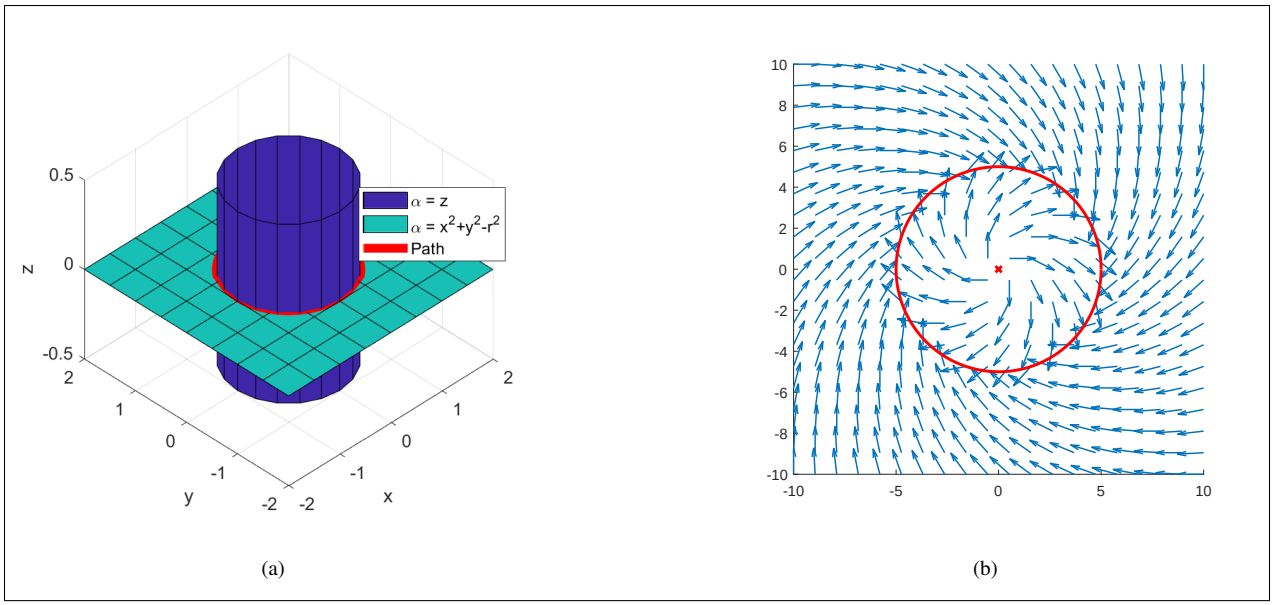

Fig. 3 GVF converging and circulating circular path

GVF was compared against LVP in a standoff tracking scenario in [Wilhelm] where a fixed wing UAV was tasked with with loitering around a moving ground target while avoiding static obstacles. A circular time-varying attractive vector field was attached to a moving ground target. Static circular repulsive vector fields centered at the obstacles and weighted by hyperbolic tangent decay functions were summed with the attractive circular field to produce a target loitering and obstacle avoidance guidance. The performance of Lyapunov [21] and gradient vector field [24–26] were compared for their cross track error with respect to the loiter circle. Gradient vector field had favorable performance due to compensation for a time-varying vector field. The gradient vector field technique also has the benefit of decoupled weighting parameters for convergence, circulation, and time-varying terms, allowing for easy modification of field behavior.

Decay functions for avoidance fields using GVF were investigated in [Zhu] for obstacles present on a straight path. When summing attractive and repulsive vector fields there is the possibility of guidance singularities, where magnitude and direction are equal and opposite. The presence of singularities were not addressed in [Wilhelm] and [Zhu], mentioned briefly in [18] and observed in [29]. For fixed wing UAVs the lack of guidance may prevent the UAV from avoiding an obstacle, while multi-rotor UAVs may end up in a trap situation. Singularities may be present at any location where a goal field and obstacle field are of equal strength.

F. Dubins Vehicle

Dubin's vehicle's position $\overrightarrow{X}$ at time t is calculated from the integral of the velocity vector $\overrightarrow{U}$. The vehicle has a constant velocity magnitude u_{uav} at a heading θ. The rate at which θ changes with respect to time is based on limitations of the craft itself.

$$\overrightarrow{U}(t) = u_{uav} \begin{bmatrix} cos(\theta(t)) \\ sin(\theta(t)) \end{bmatrix} \tag{18}$$

$$\overrightarrow{X}(t) = \overrightarrow{U} dt + \overrightarrow{X}(t-1) \tag{19}$$

$$\dot{\theta} \leq 20 deg/s \tag{20}$$

III. methods

Overview of methods
Construction of guidance for desired path
Construction of avoidance guidance
Path following and obstacle avoidance guidance
Singularity detection
Selection of vf parameters for optimized obstacle avoidance

A. Path Following with GVF

Path following guidance for a planar UAV at position (x, y) for a time invariant line is achieved by summing together convergence $\overrightarrow{V}_{conv}$ and circulation $\overrightarrow{V}_{circ}$ terms shown in Equation **??**.

where the plane defined by implicit surface function α_1 is at angle δ and plane α_2 is at constant height of $Z = 1$ shown in Equations 21 and 22 respectively.

$$\alpha_1 = cos(\delta)x + sin(\delta)y \tag{21}$$

$$\alpha_2 = z \tag{22}$$

The gradient ∇ of the potential function V is shown in Equation 23.

$$\nabla V = -\frac{1}{2(\sqrt{\cos^2(\delta)x^2 + 2\cos(\delta)\sin(\delta)xy + \sin^2(\delta)y^2})} \begin{bmatrix} 2x\cos^2(\delta) + 2\cos(\delta)\sin(\delta)y \\ 2y\sin^2(\delta) + 2\cos(\delta)\sin(\delta)x \\ 2 \end{bmatrix} \tag{23}$$

Circulation is calculated by the cross product of the surface function gradients, shown in Equation **??** and 24.

$$\overrightarrow{V}_{circ} = \begin{bmatrix} sin(\theta) \\ -cos(\theta) \\ 0 \end{bmatrix} \tag{24}$$

Guidance for a path at angle $\delta = 0$ and equal parts circulation and convergence weights $G = H = 1$ is shown in Figure 4 below.

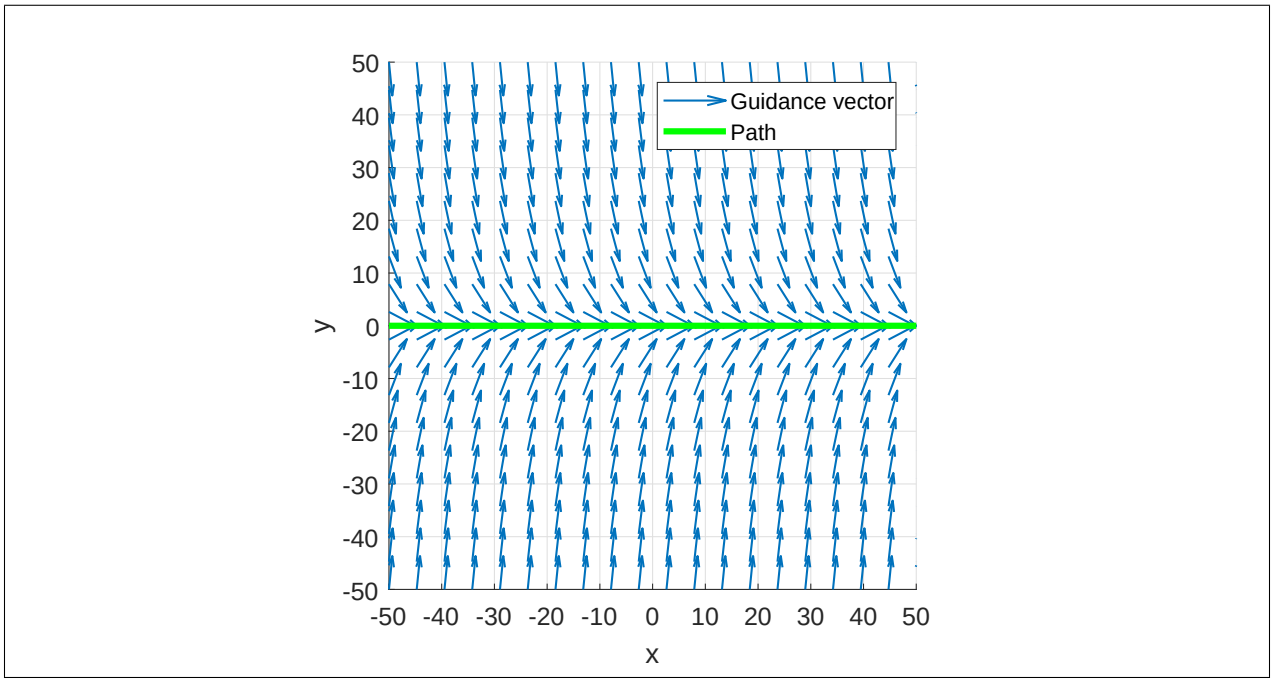

Fig. 4

B. Avoidance

Constructing a repulsive vector field for avoidance using the GVF method starts with constructing a vector field that converges and circulates a circular path. A GVF that converges and circulates a circular path is constructed with the implicit functions of a cylinder of radius r centered at (x_c, y_c) and a level plane of constant height Z, shown in Equations 25 and 26 below.

$$\alpha_1 = (x - x_c)^2 + (y - y_c)^2 - r^2 \tag{25}$$

$$\alpha_2 = z \tag{26}$$

Convergence is determined by the gradient of the potential function 23, which when simplified evaluates to

$$\vec{V}_{conv} = A\vec{B} \tag{27}$$

where

$$A = \frac{-1}{\sqrt{\bar{x}^4 + \bar{y}^4 + 2\bar{x}^2\bar{y}^2 - 2r^2\bar{x}^2 - 2r^2\bar{y}^2 + r^2 + z^2}} \tag{28}$$

and

$$\vec{B} = \begin{bmatrix} 2\bar{x}^3 + 2\bar{x}\bar{y}^2 - 2r^2\bar{x} \\ 2\bar{y}^3 + 2\bar{x}^2\bar{y} - 2r^2\bar{y} \\ z \end{bmatrix} \tag{29}$$

.

$$\bar{x} = x - x_c \tag{30}$$

$$\bar{y} = y - y_c \tag{31}$$

Circulation is calculated from the cross product of each implicit surface functions gradient, which simplifies to

$$\overrightarrow{V}_{circ} = \begin{bmatrix} 2(y - y_c) \\ -2(x - x_c) \\ 0 \end{bmatrix} \tag{32}$$

Guidance for avoiding a circular path with a large radius can be produced by setting the convergence weight $G = -1$ and circulation weight $H = 0$, shown in Figure 5. Note that the vectors are normalized prior to applying decay to ensure the vector field strength is bounded.

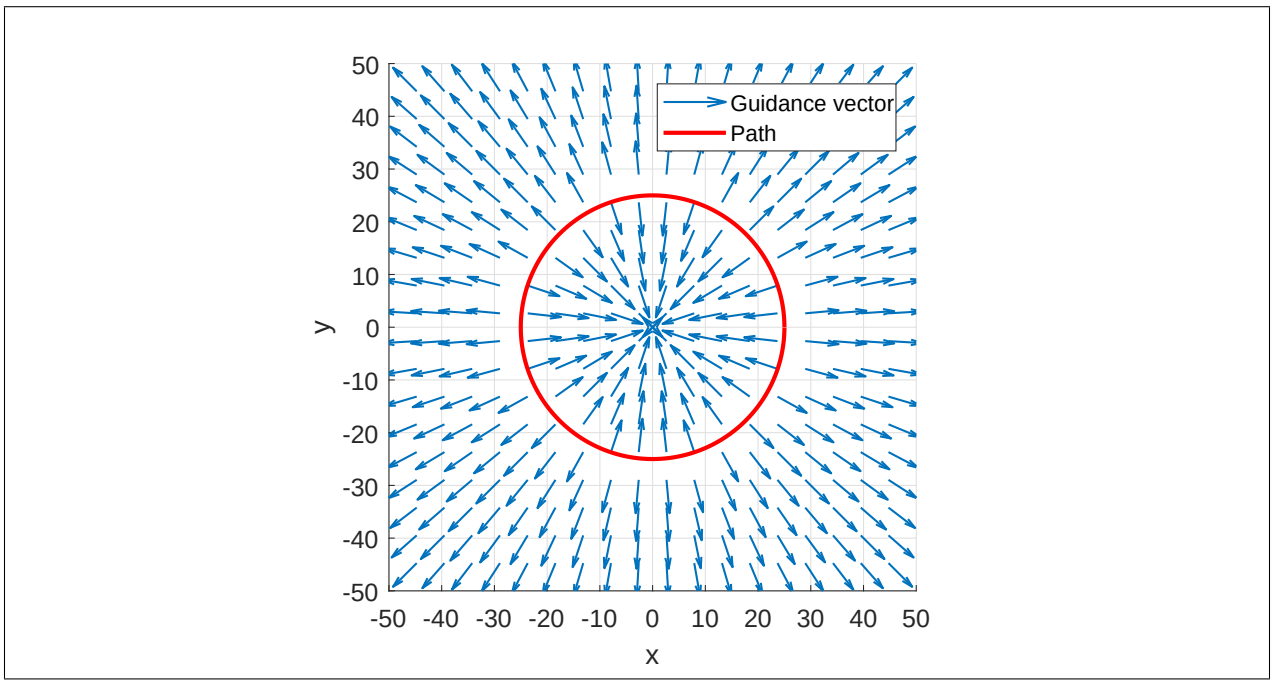

Fig. 5

Note that inside of the path, vectors point towards the center of the circle which may produce a trap situation if the UAV ends up inside the radius. To prevent a trap situation inside of the circular path, the radius of the path can be reduced, as shown in Figure 6 where $r = 0.01$.

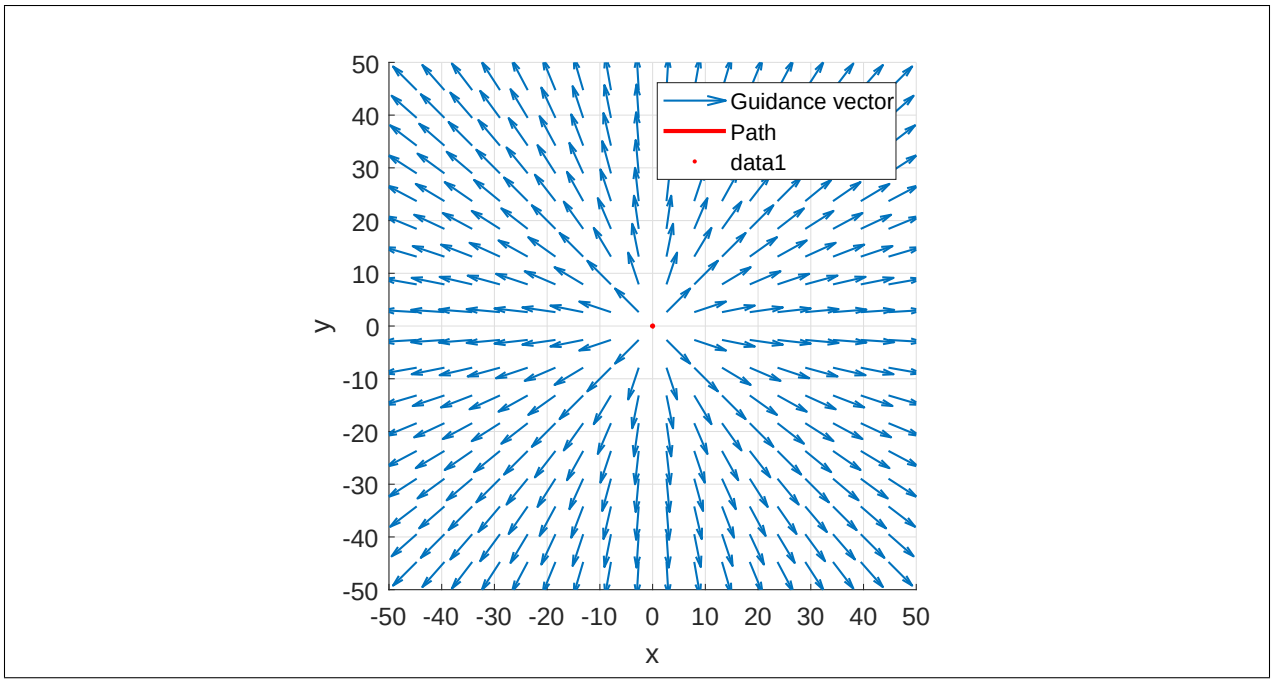

Fig. 6

To limit the influence of the repulsive field to a radius R, a decay function is applied prior to summing with the path following guidance. The decay strength P is determined in 33, where d is the euclidean distance, or range, between the UAV and the center of the obstacle, shown in Equation 34. At a distance $d > R$ the decay strength P is effectively zero, having virtual no influence on the total guidance. At a distance $d \leq R$, the field strength is bounded between $[0, 2]$.

$$P = -\tanh\left(\frac{2\pi d}{R} - \pi\right) + 1 \tag{33}$$

$$d = \sqrt{\bar{x}^2 + \bar{y}^2} \tag{34}$$

Applying the decay function with a decay edge radius $R = 35$ to the GVF shown in figure 6, results in the field shown in Figure 7.

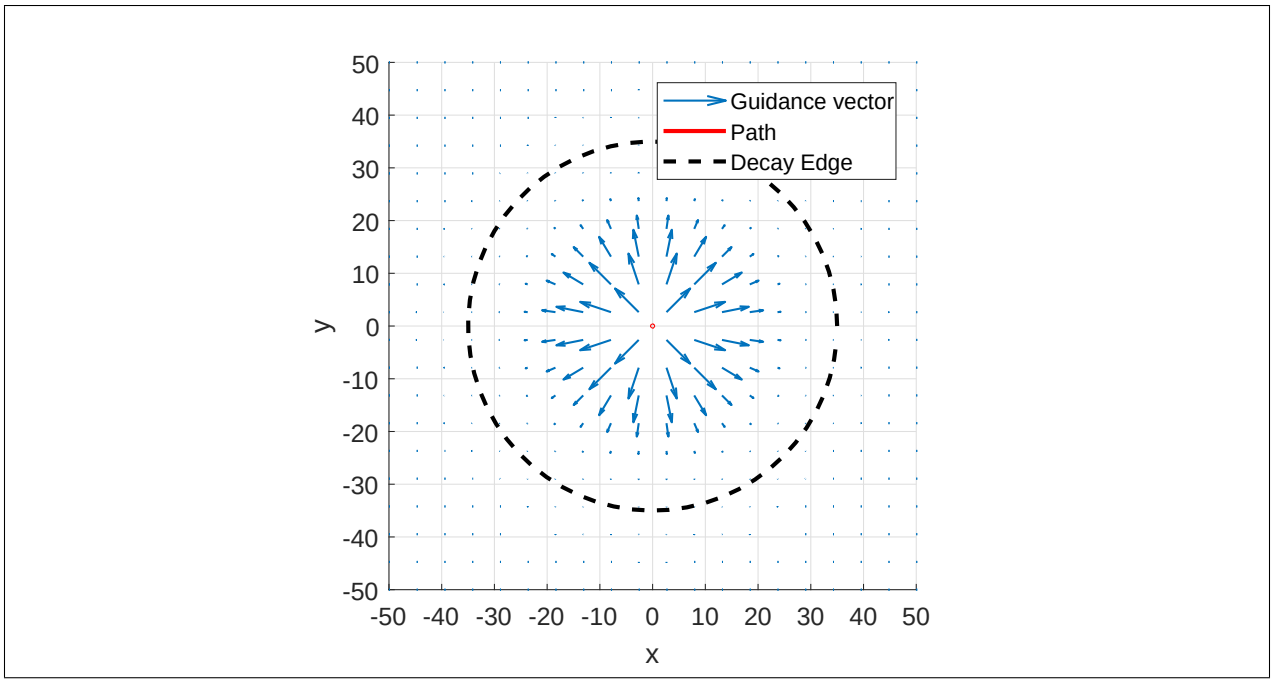

Fig. 7

Summing together the path following field with an obstacle centered on the path results in the guidance $\vec{V}_G$ shown in Figure 8.

$$\vec{V}_g = \vec{V}_{path} + P\vec{V}_{obst} \tag{35}$$

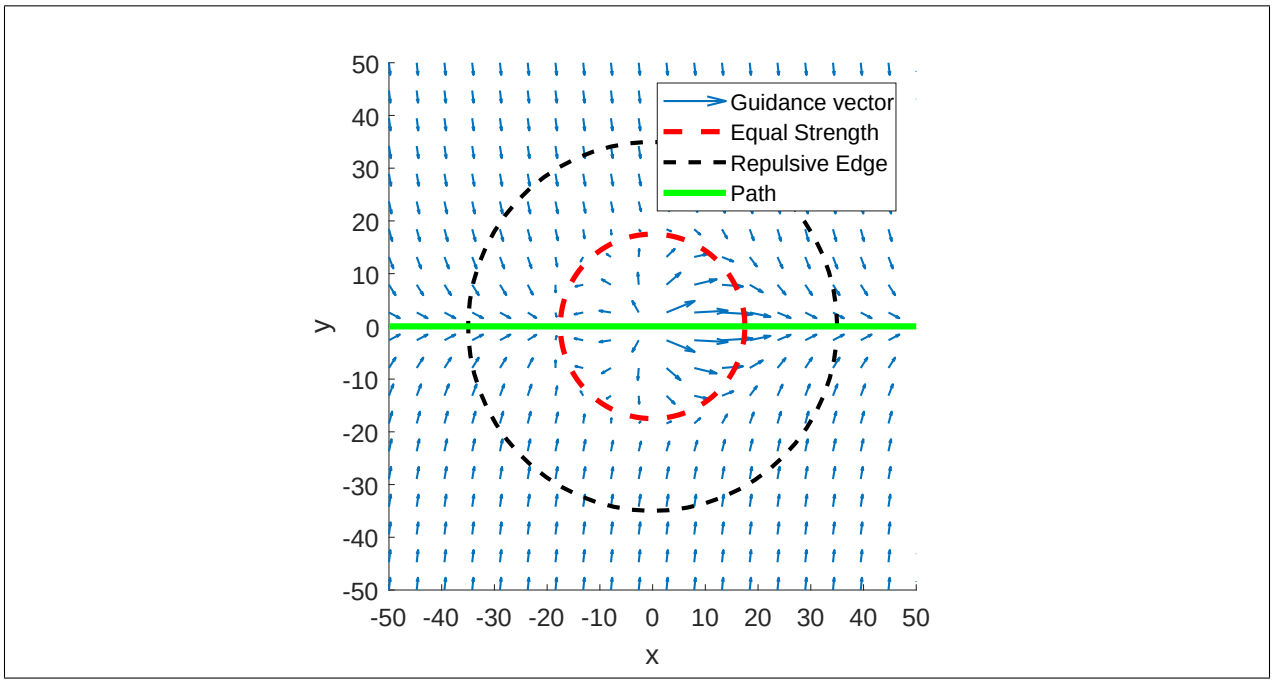

Fig. 8

C. Singularity Detection

$$||\overrightarrow{V}_g|| = 0 \tag{36}$$

Summing GVFs together may lead to small regions where the vector magnitude is near or equal to zero. Singularities are expected to exist where two summed fields have equal strength. The location of the singularities can be found by determining where the magnitude of the resulting guidance is equal to zero.

Plotting the magnitude of the summed field near the obstacle shows a well that descends into several local minimums called singularities, shown in Figure 9.

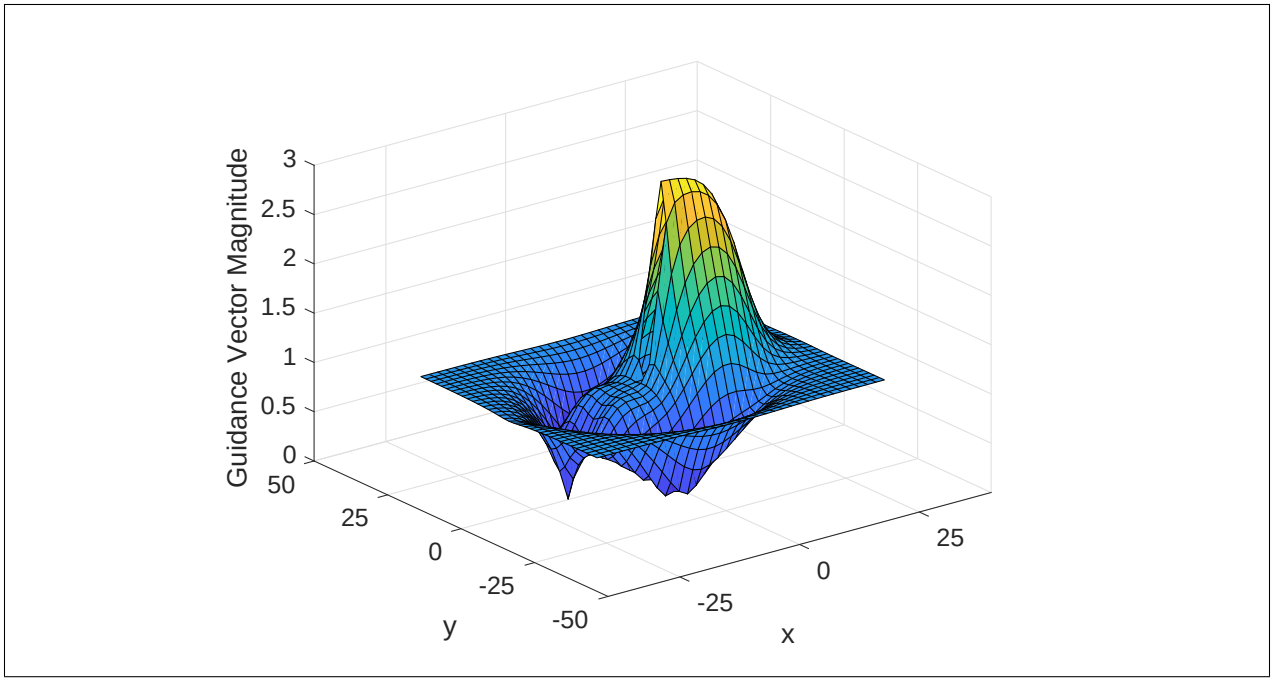

Fig. 9

Multiple singularities or near zero guidance regions may exist, so several initial conditions must be evaluated to increase the probability of detection. With the path and obstacle field shown in 8, several initial conditions evenly spaced were evaluated both inside and outside of the equal strength circle. Note how only points left of the obstacle were evaluated since this region is where attractive and repulsive vectors oppose each other, therefore it is where singularities are expected. Both inside and outside initial conditions determine the location of the singularities.

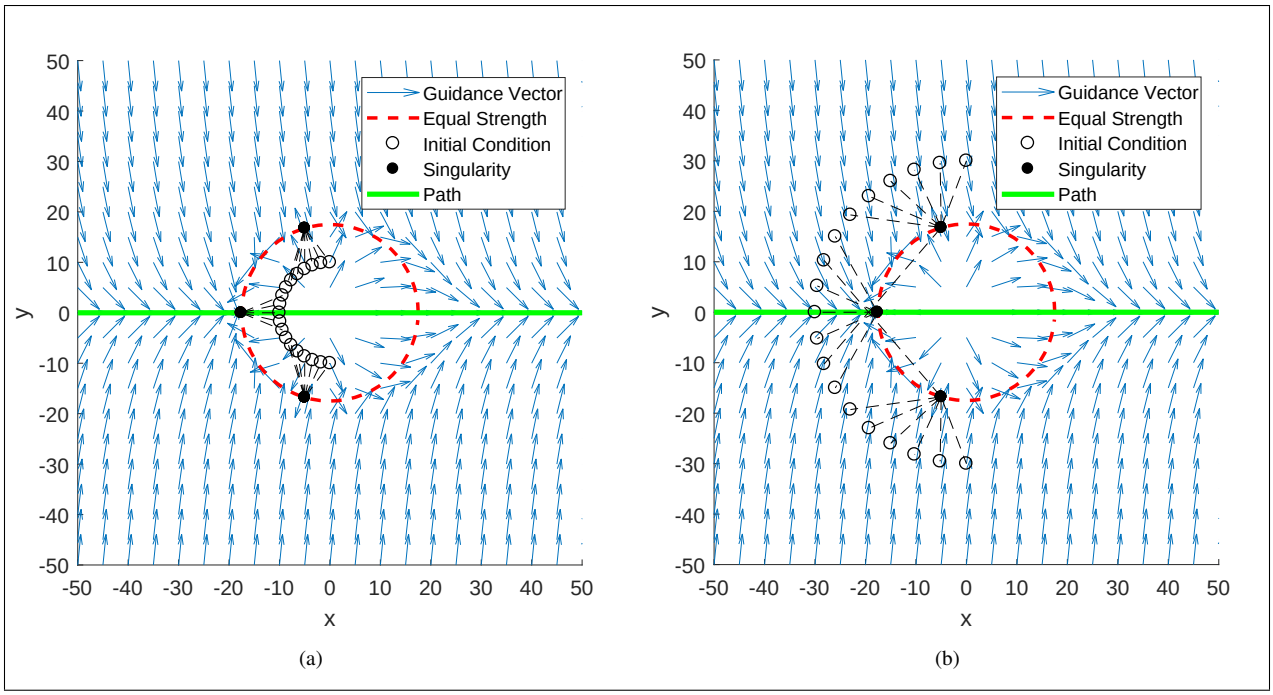

Fig. 10 GVF converging and circulating circular path

D. Flight Envelope

Evaluating a large number of initial conditions to improve the probability of finding singularities may be computationally expensive and may also find singularities the UAV may not encounter. Selecting a reduced set of initial conditions and to determine if the singularities exist where the UAV may fly, a flight envelope is determined for some time horizon t_h. Consider the UAV depicted in Figure 11 with a turn rate $\dot{\theta}$ and fixed speed u.

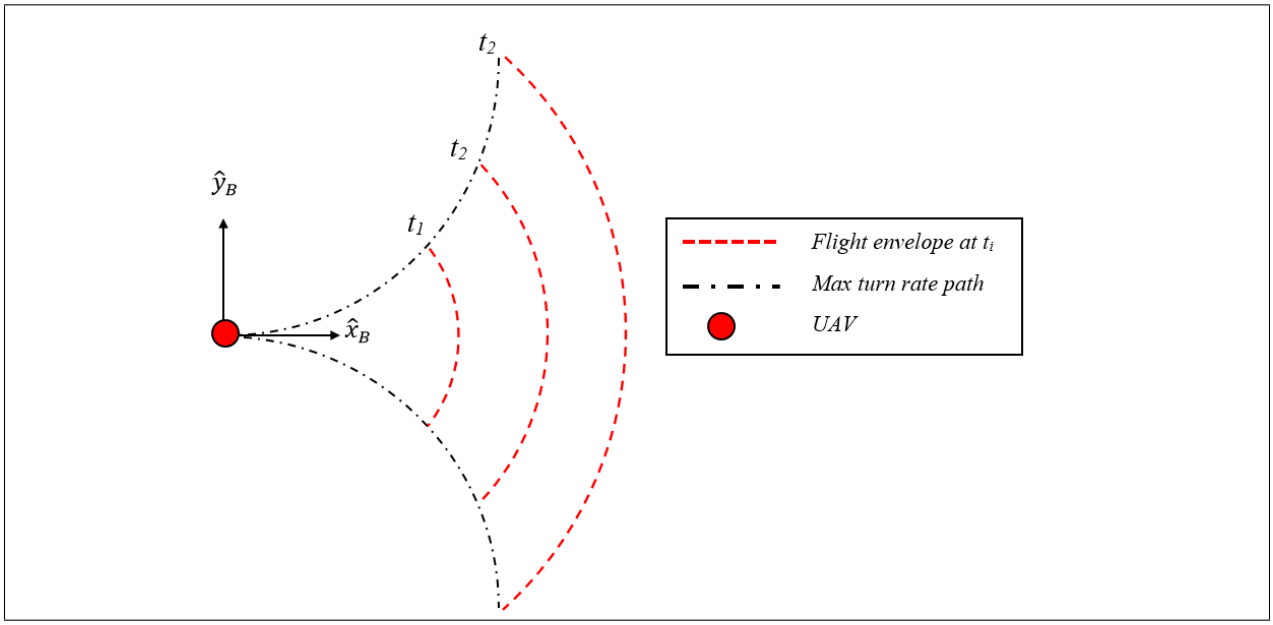

Fig. 11

The flight envelope, or positions the UAV, at time t_i with respect to the body frame is calculated in Equations 37 and 38

$$q_x = \frac{u}{\dot{\theta}} \sin(t_h \dot{\theta}) \tag{37}$$

$$q_y = \frac{u}{\dot{\theta}} \left(1 - \cos(t_h \dot{\theta})\right) \tag{38}$$

It is convenient to represent points on the flight envelope in the global inertial frame. The flight envelope points (q_x, q_y) can be expressed in vector form by finding the angle ϕ with respect to the body frame $\hat{x}_b$ axis and the vector magnitude q shown in equations 39 and 40 respectively.

$$\phi = \tan^{-1}\left(\frac{q_y}{q_x}\right) \tag{39}$$

$$q = \sqrt{q_x^2 + q_y^2} \tag{40}$$

$$\overrightarrow{Q_b} = \begin{bmatrix} q\cos\phi \\ q\sin\phi \\ 0 \end{bmatrix} \tag{41}$$

To express the flight envelope in the global inertial frame, the position vector of the UAV $\overrightarrow{P}_0$ and θ are applied with a rotation matrix R, shown in Equations 44, 42, and 43 below.

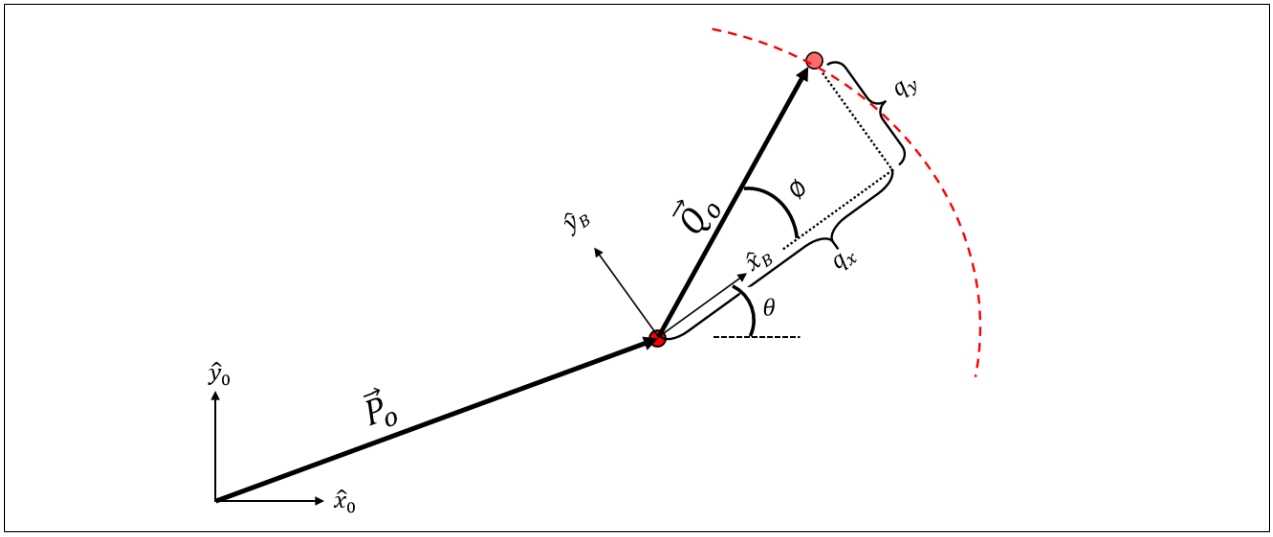

Fig. 12

$$\overrightarrow{P}_0 = \begin{bmatrix} x & y & 0 \end{bmatrix}^T \tag{42}$$

$$R = \begin{bmatrix} \cos(\theta) & -\sin(\theta) & 0 \\ \sin(\theta) & \cos(\theta) & 0 \\ 0 & 0 & 1 \end{bmatrix} \tag{43}$$

$$\overrightarrow{Q}_0 = \overrightarrow{P}_0 + R\overrightarrow{Q_b} \tag{44}$$

Initial conditions placed on the flight envelope will follow the magnitude gradient of the GVF guidance and locate any singularities it may encounter. When a singularity is found to exist inside or near a flight envelope the field can be modified to counteract it.

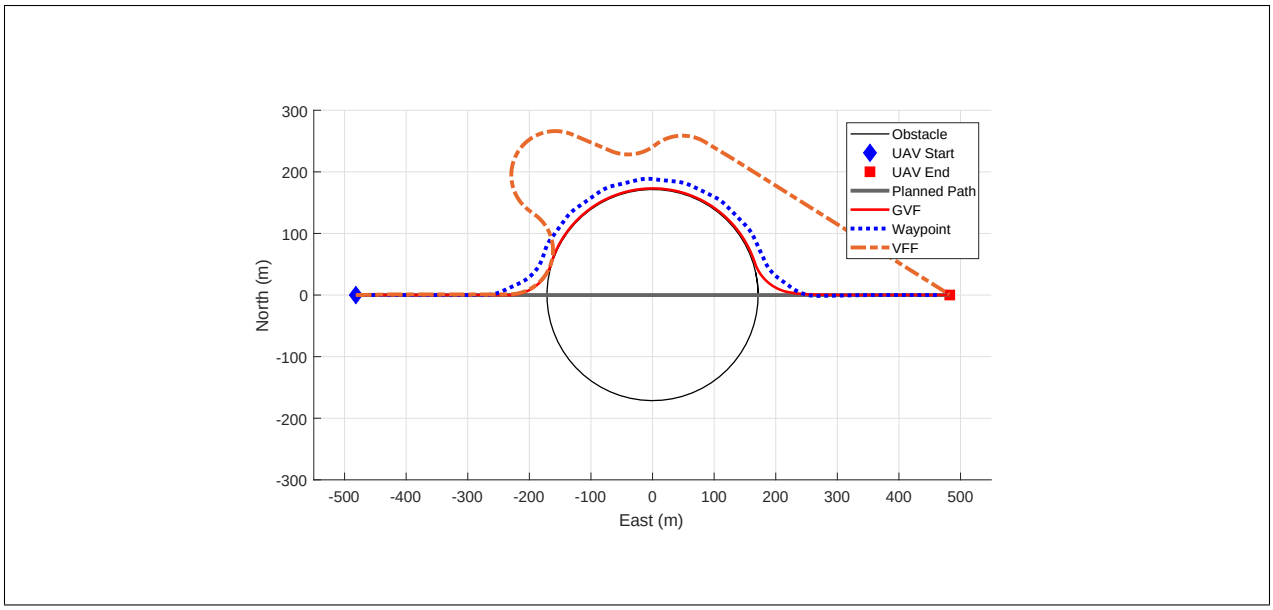

Fig. 13

IV. Simulations

V. Conclusion

Method	Cost (-)	RMS Error (m)
Waypoint	16.34	16.75
VFF	34.87	91.65
GVF	13.79	1.65

Appendix

Acknowledgments

References

[1] Ariyur, K. B., and Fregene, K. O., "Autonomous tracking of a ground vehicle by a UAV," *American Control Conference, 2008*, IEEE, 2008, pp. 669–671.

[2] Teuliere, C., Eck, L., and Marchand, E., "Chasing a moving target from a flying UAV," *Intelligent Robots and Systems (IROS), 2011 IEEE/RSJ International Conference on*, IEEE, 2011, pp. 4929–4934.

[3] Oh, H., Kim, S., Shin, H.-S., Tsourdos, A., and White, B., "Coordinated standoff tracking of groups of moving targets using multiple UAVs," *Control & Automation (MED), 2013 21st Mediterranean Conference on*, IEEE, 2013, pp. 969–977. URL `http://ieeexplore.ieee.org/abstract/document/6608839/`.

[4] Hyondong Oh, Seungkeun Kim, Hyo-sang Shin, and Tsourdos, A., "Coordinated standoff tracking of moving target groups using multiple UAVs," *IEEE Transactions on Aerospace and Electronic Systems*, Vol. 51, No. 2, 2015, pp. 1501–1514. doi:10.1109/TAES.2015.140044, URL `http://ieeexplore.ieee.org/document/7126199/`.

[5] Ulun, S., and Unel, M., "Coordinated motion of UGVs and a UAV," *Industrial Electronics Society, IECON 2013-39th Annual Conference of the IEEE*, IEEE, 2013, pp. 4079–4084. URL `http://ieeexplore.ieee.org/abstract/document/6699789/`.

[6] Wilhelm, J., Clem, G., and Eberhart, G., "Direct Entry Minimal Path UAV Loitering Path Planning," *Aerospace*, Vol. 4, No. 2, 2017, p. 23. doi:10.3390/aerospace4020023, URL `http://www.mdpi.com/2226-4310/4/2/23`.

[7] Khatib, O., "Real-time obstacle avoidance for manipulators and mobile robots," *The international journal of robotics research*, Vol. 5, No. 1, 1986, pp. 90–98. URL http://journals.sagepub.com/doi/abs/10.1177/027836498600500106.

[8] Rimon, E., "Exact Robot Navigation Using Artificial Potential Functions.pdf," , 1992.

[9] Borenstein, J., and Koren, Y., "Real-time obstacle avoidance for fast mobile robots in cluttered environments," *Robotics and Automation, 1990. Proceedings., 1990 IEEE International Conference on*, IEEE, 1990, pp. 572–577. URL http://ieeexplore.ieee.org/abstract/document/126042/.

[10] Borenstein, J., and Koren, Y., "The vector field histogram-fast obstacle avoidance for mobile robots," *IEEE transactions on robotics and automation*, Vol. 7, No. 3, 1991, pp. 278–288. URL http://ieeexplore.ieee.org/abstract/document/88137/.

[11] Koren, Y., and Borenstein, J., "Potential Field Methods and their inherent limitions for morbile robot navigation.pdf," , 1991. URL http://ieeexplore.ieee.org/document/131810/.

[12] Liu, Y., and Zhao, Y., "A virtual-waypoint based artificial potential field method for UAV path planning," *Guidance, Navigation and Control Conference (CGNCC), 2016 IEEE Chinese*, IEEE, 2016, pp. 949–953. URL http://ieeexplore.ieee.org/abstract/document/7828913/.

[13] Kim, D. H., "Escaping route method for a trap situation in local path planning," *International Journal of Control, Automation and Systems*, Vol. 7, No. 3, 2009, pp. 495–500. doi:10.1007/s12555-009-0320-7, URL http://link.springer.com/10.1007/s12555-009-0320-7.

[14] Goerzen, C., Kong, Z., and Mettler, B., "A Survey of Motion Planning Algorithms from the Perspective of Autonomous UAV Guidance," *Journal of Intelligent and Robotic Systems*, Vol. 57, No. 1-4, 2010, pp. 65–100. doi:10.1007/s10846-009-9383-1, URL http://link.springer.com/10.1007/s10846-009-9383-1.

[15] Lei Tang, Songyi Dian, Gangxu Gu, Kunli Zhou, Suihe Wang, and Xinghuan Feng, "A novel potential field method for obstacle avoidance and path planning of mobile robot," IEEE, 2010, pp. 633–637. doi:10.1109/ICCSIT.2010.5565069, URL http://ieeexplore.ieee.org/document/5565069/.

[16] Li, G., Yamashita, A., Asama, H., and Tamura, Y., "An efficient improved artificial potential field based regression search method for robot path planning," IEEE, 2012, pp. 1227–1232. doi:10.1109/ICMA.2012.6283526, URL http://ieeexplore.ieee.org/document/6283526/.

[17] Sujit, P., Saripalli, S., and Sousa, J. B., "Unmanned Aerial Vehicle Path Following: A Survey and Analysis of Algorithms for Fixed-Wing Unmanned Aerial Vehicless," *IEEE Control Systems*, Vol. 34, No. 1, 2014, pp. 42–59. doi:10.1109/MCS.2013.2287568, URL http://ieeexplore.ieee.org/document/6712082/.

[18] Nelson, D. R., "Cooperative control of miniature air vehicles," 2005. URL http://scholarsarchive.byu.edu/etd/1095/.

[19] Nelson, D. R., Barber, D. B., McLain, T. W., and Beard, R. W., "Vector field path following for small unmanned air vehicles," *American Control Conference, 2006*, IEEE, 2006, pp. 7–pp. URL http://ieeexplore.ieee.org/abstract/document/1657648/.

[20] Nelson, D., Barber, D., McLain, T., and Beard, R., "Vector Field Path Following for Miniature Air Vehicles," *IEEE Transactions on Robotics*, Vol. 23, No. 3, 2007, pp. 519–529. doi:10.1109/TRO.2007.898976, URL http://ieeexplore.ieee.org/document/4252175/.

[21] Frew, E. W., "Cooperative standoff tracking of uncertain moving targets using active robot networks," *Robotics and Automation, 2007 IEEE International Conference on*, IEEE, 2007, pp. 3277–3282. URL http://ieeexplore.ieee.org/abstract/document/4209596/.

[22] Miao, Z., Thakur, D., Erwin, R. S., Pierre, J., Wang, Y., and Fierro, R., "Orthogonal vector field-based control for a multi-robot system circumnavigating a moving target in 3D," *Decision and Control (CDC), 2016 IEEE 55th Conference on*, IEEE, 2016, pp. 6004–6009. URL http://ieeexplore.ieee.org/abstract/document/7799191/.

[23] Griffiths, S., "Vector Field Approach for Curved Path Following for Miniature Aerial Vehicles," American Institute of Aeronautics and Astronautics, 2006. doi:10.2514/6.2006-6467, URL http://arc.aiaa.org/doi/10.2514/6.2006-6467.

[24] Goncalves, V. M., Pimenta, L. C. A., Maia, C. A., and Pereira, G. A. S., "Artificial vector fields for robot convergence and circulation of time-varying curves in n-dimensional spaces," IEEE, 2009, pp. 2012–2017. doi:10.1109/ACC.2009.5160350, URL http://ieeexplore.ieee.org/document/5160350/.

[25] Gonçalves, V. M., Pimenta, L. C., Maia, C. A., Pereira, G. A., Dutra, B. C., Michael, N., Fink, J., and Kumar, V., "Circulation of curves using vector fields: actual robot experiments in 2D and 3D workspaces," *Robotics and Automation (ICRA), 2010 IEEE International Conference on*, IEEE, 2010, pp. 1136–1141.

[26] Gonçalves, V. M., Pimenta, L. C., Maia, C. A., Dutra, B. C., and Pereira, G. A., "Vector fields for robot navigation along time-varying curves in $ n $-dimensions," *IEEE Transactions on Robotics*, Vol. 26, No. 4, 2010, pp. 647–659. URL http://ieeexplore.ieee.org/abstract/document/5504176/.

[27] Gerlach, A. R., *Autonomous Path-Following by Approximate Inverse Dynamics and Vector Field Prediction*, University of Cincinnati, 2014. URL http://search.proquest.com/openview/432d738d856bf0a9b46acea1b1eee08f/1?pq-origsite=gscholar&cbl=18750&diss=y.

[28] Jung, W., Lim, S., Lee, D., and Bang, H., "Unmanned Aircraft Vector Field Path Following with Arrival Angle Control," *Journal of Intelligent & Robotic Systems*, Vol. 84, No. 1-4, 2016, pp. 311–325. doi:10.1007/s10846-016-0332-5, URL http://link.springer.com/10.1007/s10846-016-0332-5.

[29] Panagou, D., "Motion planning and collision avoidance using navigation vector fields," *Robotics and Automation (ICRA), 2014 IEEE International Conference on*, IEEE, 2014, pp. 2513–2518. URL http://ieeexplore.ieee.org/abstract/document/6907210/.